A Role for *Epha2* in Cell Migration and Refractive Organization of the Ocular Lens

Yanrong Shi, Alicia De Maria, Thomas Bennett, Alan Shiels, and Steven Bassnett

Purpose. The Epha2 receptor is a surprisingly abundant component of the membrane proteome of vertebrate lenses. In humans, genetic studies have linked mutations in *EPHA2* to inherited and age-related forms of cataract, but the function of Epha2 in the lens is obscure. To gain insights into the role of Epha2, a comparative analysis of lenses from wild-type and *Epha2*$^{-/-}$ mice was performed.

Methods. Epha2 distribution was examined using immunocytochemistry and Western blot analysis. Lens optical quality was assessed by laser refractometry. Confocal microscopy was used to analyze cellular phenotypes.

Results. In wild-type lenses, Epha2 was expressed by lens epithelial cells and elongating fibers but was degraded during the later stages of fiber differentiation. Epha2-null lenses retained their transparency, but two key optical parameters, lens shape and internal composition, were compromised in *Epha2*$^{-/-}$ animals. Epha2-null lenses were smaller and more spherical than age-matched wild-type lenses, and laser refractometry revealed a significant decrease in refractive power of the outer cell layers of mutant lenses. In the absence of Epha2, fiber cells deviated from their normal course and terminated at sutures that were no longer centered on the optical axis. Patterning defects were also noted at the level of individual cells. Wild-type fiber cells had hexagonal cross-sectional profiles with membrane protrusions extending from the cell vertices. In contrast, *Epha2*$^{-/-}$ cells had irregular profiles, and protrusions extended from all membrane surfaces.

Conclusions. These studies indicate that Epha2 is not required for transparency but does play an indispensable role in the cytoarchitecture and refractive quality of the lens. (*Invest Ophthalmol Vis Sci.* 2012;53:551–559) DOI:10.1167/iovs.11-8568

The Eph receptors constitute the largest subfamily of receptor tyrosine kinases.[1] The extracellular domains of Eph receptors interact with membrane-bound ligands, ephrins, located on the surfaces of adjacent cells. Unlike other receptor tyrosine kinases, Eph receptors function primarily in the regulation of cell shape, cell-substrate adhesion, and migration, though in certain contexts Eph receptors can also influence proliferation.[2]

Eph receptors take their name from the erythropoietin-producing hepatocellular carcinoma cell line from which the first member of the family, EPHA1, was cloned.[3] Eph receptors are divided into A and B subclasses.[4] In mammals, nine Epha (Epha1–8 and Epha10) and five Ephb (Ephb1–4 and Ephb6) receptors are known. Ephrin ligands are also classified into two groups: ephrin-a ligands (Efna1–5 in mammals) are GPI-linked proteins, whereas ephrin-b ligands (Efnb1–3) are transmembrane proteins. Typically, EphA receptors bind to ephrin-A ligands and EphB receptors bind to ephrin-B ligands, although limited cross-talk between class members has been reported.[5] Eph-ephrin binding is unusual in that it can stimulate bidirectional signaling: forward signaling into the receptor-expressing cell and reverse signaling into the ligand-expressing cell.[2]

As a group, Eph receptors are expressed most prominently during development, when they play critical roles in such processes as limb formation and nervous system patterning. Most Eph receptors are expressed at low levels in adult tissues. A notable exception to this is Epha2 (originally called Eck, for epithelial cell kinase), which was cloned from HeLa cells[6] and was shown to be enriched in adult tissues with high epithelial content such as lung, digestive tract, and skin.[7] The biology of Epha2 has been studied intensively because the receptor is overexpressed in many human cancers.[8–10]

Recent studies have identified Epha2 as a surprisingly abundant plasma membrane component in cells of the ocular lens.[11] The precise role of Epha2 in the lens is unknown, but mutations in *EPHA2* have been shown to underlie inherited forms of cataract in humans.[12–14] Moreover, common variants in E*PHA2* have been associated with the much more prevalent age-related form of cataract.[12,15,16] To gain insights into the role of Epha2 in the lens, we analyzed the lens phenotype of *Epha2*-null mice. Our data suggest that *Epha2* is not required for lens transparency but does play a significant role in cell guidance and refractive organization of the lens.

Materials and Methods

Animals

Epha2$^{-/-}$ mice (strain name, C57BL/6;129S6-Epha2^{tm1Jrui}; stock number, 006028) were obtained from The Jackson Laboratory (Bar Harbor, ME) on a C57BL/6;129S6 mixed background.[17] Molecular analysis of the Epha2 locus confirmed that the targeting vector was inserted into exon 5, resulting in predicted termination of protein translation at an in-frame translation stop-codon (TGA) located 85 codons downstream within the targeting vector (Supplementary Fig. S1 and Supplementary Table S1, http://www.iovs.org/lookup/suppl/doi:10.1167/iovs.11-8568/-/DCSupplemental). *Epha2*$^{-/-}$ males were crossed with C57BL/6J females to eliminate the 6-kb deletion in the gene for lens beaded-filament structural protein-2 (*Bfsp2*) that is characteristic of the 129 strain.[18] PCR genotyping was used to identify *Epha2*$^{-/-}$ progeny that were homozygous for the wild-type *Bfsp2* allele before colony expansion (data not shown). Age-matched C57BL/6 mice were used as

From the Department of Ophthalmology and Visual Sciences, Washington University School of Medicine, St. Louis, Missouri.

Supported by National Institutes of Health Grants EY018185 (SB), EY09852 (SB), and EY012284 (AS) and Core Grant for Vision Research P30EY02687; an unrestricted grant to the Department of Ophthalmology and Visual Sciences from Research to Prevent Blindness; and a Research to Prevent Blindness Wasserman award (SB).

Submitted for publication September 9, 2011; revised November 17, 2011; accepted November 18, 2011.

Disclosure: **Y. Shi**, None; **A. De Maria**, None; **T. Bennett**, None; **A. Shiels**, None; **S. Bassnett**, None

Corresponding author: Steven Bassnett, Department of Ophthalmology and Visual Sciences, Washington University School of Medicine, 660 S. Euclid Avenue, Campus Box 8096, St. Louis, MO 63110; bassnett@vision.wustl.edu.

Copyright 2012 The Association for Research in Vision and Ophthalmology, Inc.

controls in this study. A limited number of C57BL/6;129S6 animals (i.e., the original mixed background strain) were also examined and were found to be phenotypically indistinguishable from C57BL/6 mice.

Animals were killed by CO_2 inhalation. Eyes were enucleated, and lenses were removed through an incision in the posterior of the eye globe. All procedures described herein were approved by the Washington University Animal Studies Committee and were performed in accordance with the ARVO Statement for the Use of Animals in Ophthalmic and Vision Research.

Isolation of Proteins from Different Lens Strata

The tissue distribution of Epha2 was determined using a progressive lysis technique in which proteins were isolated from various lens strata, as described.[19] Pools of 8–10 decapsulated lenses from wild-type mice were dissolved with stirring in 300 μL lysis buffer (50 mM Tris-HCl, pH 7.4, 1% SDS) containing protease inhibitor cocktail (Roche Applied Science, Indianapolis, IN). Samples were withdrawn at intervals, and protein content was determined by BCA assay (Bio-Rad, Hercules, CA).

Immunoblot Analysis

Proteins (50 μg) were separated by SDS-PAGE on 4%–12% Bis-Tris gradient gels (NuPAGE; Invitrogen, Carlsbad, CA) and transferred to nitrocellulose. Blots were probed with rabbit anti-mouse EphA2 (sc-924; Santa Cruz Biotechnology, Inc., Santa Cruz, CA). To locate the border of the lens organelle-free zone (OFZ), blots were reprobed with an antibody against a mitochondrial protein (succinate-ubiquinone reductase; A11142; Invitrogen). Primary antibodies were detected using horseradish peroxidase-conjugated secondary antibodies (Thermo Fisher Scientific, Rockford, IL) and chemiluminescence.

Immunofluorescence

Lenses were fixed for 30 minutes in 4% paraformaldehyde/PBS and then cryoprotected by sequential incubation in 5%, 10%, and 20% sucrose/PBS. Lenses were mounted in optimum temperature cutting compound (OCT; Tissue-Tek; Electron Microscopy Sciences, Hatfield, PA), frozen in a 2-methylbutane/dry ice slurry, cryosectioned at 20 μm, and collected onto poly-lysine–coated slides. Sections were permeabilized in 0.1% Triton X-100/PBS and blocked in 3% bovine serum albumin/PBS overnight. Sections were incubated overnight at 4°C in 1:100 dilution of goat anti-mouse EphA2 antibody (AF639; R&D Systems, Minneapolis, MN). After washing in PBS, sections were incubated in 1:100 dilution of Alexa 488–conjugated donkey anti-goat antibody (Invitrogen) and counterstained with 1:1000 dilution of Draq5 (Biostatus Ltd., Leicester, UK), a fluorescent DNA stain. Sections were then washed and mounted in mounting medium (Prolong; Invitrogen).

Cell Proliferation

Proliferating cells were visualized after the incorporation of 5-ethynyl-2′-deoxyuridine (EdU; Invitrogen). EdU was administered by intraperitoneal injection, as described.[20] Lenses were counterstained with Draq5 and imaged in three-dimensions by confocal microscopy, as described.[20]

Optical Analysis

To gauge their transparency and refractive properties, lenses from wild-type and *Epha2*$^{-/-}$ mice were dissected into prewarmed tissue culture medium and photographed against a grid pattern. Lenses were then transferred to a viewing chamber filled with tissue culture medium supplemented with 0.01% dry milk powder (to visualize refracted beams). Lenses were placed anterior face down, and the focused beam of a low-power helium/neon laser was oriented such that it passed through the lens equator orthogonal to the optic axis. The beam was moved in 100-μm increments across the lens. The angle of refraction and the focal length (back vertex distance) were measured as a function of beam eccentricity from digital images captured with a digital camera (SPOT; Diagnostic Imaging, Sterling Heights, MI). Measurements were made on three wild-type and three size-matched *Epha2*$^{-/-}$ lenses. Two-way ANOVA was used to assess the statistical significance of the data.

Lens Size and Shape Determination

Lens shape was documented by placing dissected lenses in warm tissue culture medium in a spectrophotometer cuvette. Lenses sink in tissue culture medium because they are denser than the medium. The outer cell layers are soft and may be compressed under the weight of the lens, leading to a distortion in shape. To offset this effect, density gradient medium (Percoll; GE Healthcare Bio-Sciences, Piscataway, NJ) was added to the bathing medium to a final concentration of 20%. In 20% density gradient medium (Percoll), the lens has near-neutral buoyancy; consequently, the tissue shape is not distorted under its own weight (Supplementary Fig. S2, http://www.iovs.org/lookup/suppl/doi:10.1167/iovs.11-8568/-/DCSupplemental). A profile view of the lens was obtained by photographing its reflection in a 45° glass prism positioned next to the cuvette. Images were recorded using a microscope (Macrofluo; Leica Microsystems, Buffalo Grove, IL) with a vertical beam path to avoid parallax error. Lens thickness and width were measured from calibrated images using image analysis software (Metamorph 7.7; Molecular Devices, Sunnyvale, CA). Similarly, the radii of curvature for the anterior and posterior lens surfaces were determined manually from the digital images. Preliminary measurements indicated that lenses from male animals were often slightly larger than from age-matched females, so all measurements were made on animals of a single gender (male).

Single-Cell Imaging

Individual fiber cells were dissected from the midcortical region of 1-month-old wild-type or *Epha2*$^{-/-}$ lenses and were visualized by confocal microscopy, as described.[19,21] Briefly, lenses were fixed in 4% paraformaldehyde for 5 hours and then bisected along the optic axis. Individual cells were teased from the mid-cortical region and dried onto polylysine-coated slides. Cells were permeabilized in 0.1% triton X-100 for 5 minutes, blocked in 3% bovine serum albumin/PBS for 30 minutes, and incubated overnight in 1:100 dilution of rabbit anti-human AQP0 (Alpha Diagnostics, San Antonio, TX). Aqp0 is the most abundant integral membrane protein of mouse lens fiber cells,[11] and Aqp0 immunofluorescence was used here to visualize the surface morphology of the dissected cells. Cells were washed in PBS and incubated in 1:200 dilution of Alexa 488–conjugated goat anti-rabbit antibody (Invitrogen). After washing, cells were mounted in anti-fade reagent (Prolong; Invitrogen) and coverslipped. Samples were imaged by confocal microscopy (LSM510; Carl Zeiss, Thornwood, NY). Three-dimensional image stacks were collected and deconvolved using a point-spread function distilled from through-focal images of 170 nm fluorescent beads (PS-Speck; Invitrogen). Images were deconvolved and rendered in three dimensions using image processing software (Huygens, version 3.7; Scientific Volume Imaging, Hilversum, The Netherlands).

Epithelial cell morphology was examined in intact, living lenses stained for 30 minutes with a vital lipophilic dye (FM 4-64; Invitrogen) and the DNA stain (Draq5, 1:1000 dilution; Invitrogen). Lenses were imaged in glass-bottomed microwell dishes (Mattek, Ashland, MA), as described.[20]

Visualizing Lens Suture Organization In Vivo and In Vitro

Lens sutures are virtual structures formed by the convergence of fiber cell tips beneath the anterior and posterior poles. In euthanized animals, the anterior suture was discernible in situ. A dissecting microscope was used to record the suture orientation relative to the superior-inferior axis of the head. In dissected lenses, the shapes of the anterior and posterior sutures were visualized by confocal microscopy after the cell membranes were stained with 1 μM FM 4-64 (Invitrogen).[22]

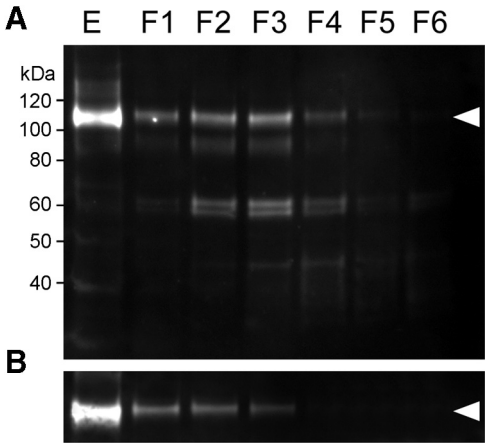

FIGURE 1. Depth-dependent expression profile of Epha2 in 1-month-old wild-type mouse lenses. (**A**) Samples were prepared from the lens epithelium (E) or progressively deeper strata of the lens (F1–F6). Full-length Epha2 (*arrowhead*) is detected in the epithelium and outer fiber layers but absent from the innermost fraction (F6). (**B**) The location of the OFZ was determined using an antibody to a mitochondrial enzyme (*arrowhead*). In this case, the border of the OFZ is located at F3 to F4.

RESULTS

Epha2 Distribution in the Lens

Epha2 expression was examined in samples isolated from various strata (F1–F6) of 1-month-old mouse lenses by progressive tissue lysis (Fig. 1). Epha2 was expressed strongly in the lens epithelium (E), as a single band of approximately 115 kDa. The same band was present, albeit at lower levels, in the outer layers of lens fiber cells (fractions F1–F4). Compared with the levels in the superficial cells (F1–F4), the full-length band was markedly reduced in intensity by F5 and absent from F6, corresponding to the innermost fiber cells. The highest levels of expression in the lens fibers were observed in fractions F2–F3 from the midcortical region of the lens. Nuclei and other organelles are degraded in the normal course of fiber cell differentiation.[23] As a result, the central region of the lens constitutes a well-demarcated OFZ. The border of the OFZ was localized on the immunoblots by reprobing with an antibody against succinate-ubiquinone reductase, a mitochondrial membrane protein. The mitochondrial marker was strongly expressed in the organelle-rich epithelium and the superficial layers of fiber cells but was not detected beyond F3, indicating that the border of the OFZ was located at F3–F4. Thus, Epha2 was expressed by epithelial cells, differentiating superficial fiber cells, and a contingent of mature fiber cells lying immediately within the OFZ. In addition to full-length (≈115 kDa) Epha2, several bands of lower molecular mass were detected in the fiber cells, including a diffuse band at ≈90 kDa and a doublet at ≈60 kDa. Many fiber cell membrane proteins are cleaved in the course of differentiation, and the lower molecular weight bands probably represented proteolytic fragments of the full-length protein. All the bands detected on the gel were likely to represent specific binding of the antibody to Epha2 because no immunopositive bands were observed on blots of lens proteins prepared from *Epha2*$^{-/-}$ mice (Supplementary Fig. S3, http://www.iovs.org/lookup/suppl/doi:10.1167/iovs.11-8568/-/DCSupplemental).

The cellular distribution of Epha2 in wild-type lenses was next visualized by indirect immunofluorescence (Fig. 2). Epha2 immunofluorescence was prominent in the membranes of epithelial cells and superficial fiber cells but was not detected in central fiber cells, consistent with the immunoblot measurements on fractionated lens samples (Fig. 1). In the fiber cells, the strongest immunofluorescence was observed in the midcortical region. All nucleated cells and a contingent of cells within the OFZ expressed Epha2. Epha2 was most abundant at the narrow faces of the fiber cell lateral membranes (Fig. 2C). As a result, the radial columns of fibers were highlighted. As expected, sections from *Epha2*$^{-/-}$ lenses exhibited only weak background staining (Fig. 2B).

Size, Shape, and Refractive Properties

Compared with age-matched wild-type lenses, *Epha2*$^{-/-}$ lenses were consistently smaller, an effect most pronounced in younger lenses (Fig. 3A). In older lenses, the anterior-posterior dimension was similar in the two genotypes, but the equatorial diameter of *Epha2*$^{-/-}$ lenses remained significantly smaller than wild-type lenses (Fig. 3B). Thus, *Epha2*$^{-/-}$ lenses were generally smaller and more spherical than age-matched wild-types. The radii of curvature of the anterior and posterior lens faces are shown in Figure 3C. In wild-type lenses, the radius of curvature of the anterior surface was consistently larger than that of the posterior surface, indicating that even under the conditions of near-neutral buoyancy achieved in these experiments, the anterior surface of the mouse lens was flatter than the posterior surface. The same relationship held in the *Epha2*$^{-/-}$ lenses.

To evaluate the transparency of lenses lacking Epha2, lenses from 8-week-old or 10-month-old wild-type and *Epha2*$^{-/-}$ mice were photographed against a regular grid pattern (Fig. 4A). All *Epha2*$^{-/-}$ lenses examined (>100 lenses) were transparent. However, refractive anomalies (noted as distortions in

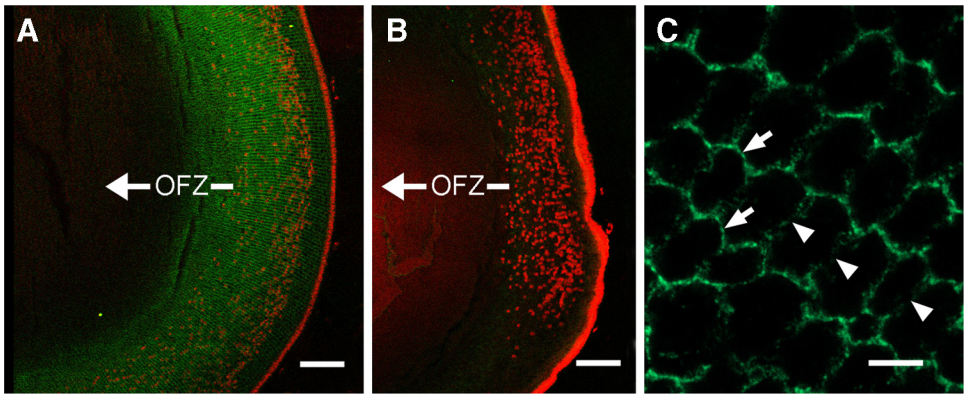

FIGURE 2. Equatorial sections of 1-month-old wild-type and *Epha2*$^{-/-}$ lenses probed with anti-Epha2 (*green*). Nuclei were stained with Draq5 (*red*). In wild-type lenses (**A**), Epha2 is detected in the epithelial layer and underlying cortical fiber cells, where the immunofluorescence delineates radial columns of fiber cells. The innermost extent of Draq5-positive nuclei marks the border of the OFZ. Epha2 immunofluorescence extends ≈100 μm into the OFZ but is not detected in the central fiber cells. Immunofluorescence is eliminated in sections prepared from *Epha2*$^{-/-}$ lenses (**B**). High-magnification images of cross-sectioned wild-type lens fiber cells (**C**) reveal that Epha2 is more abundant at the narrow membrane faces (*arrows*) than at the broad membrane faces (*arrowheads*). Scale bars: 100 μm (**A**, **B**); 5 μm (**C**).

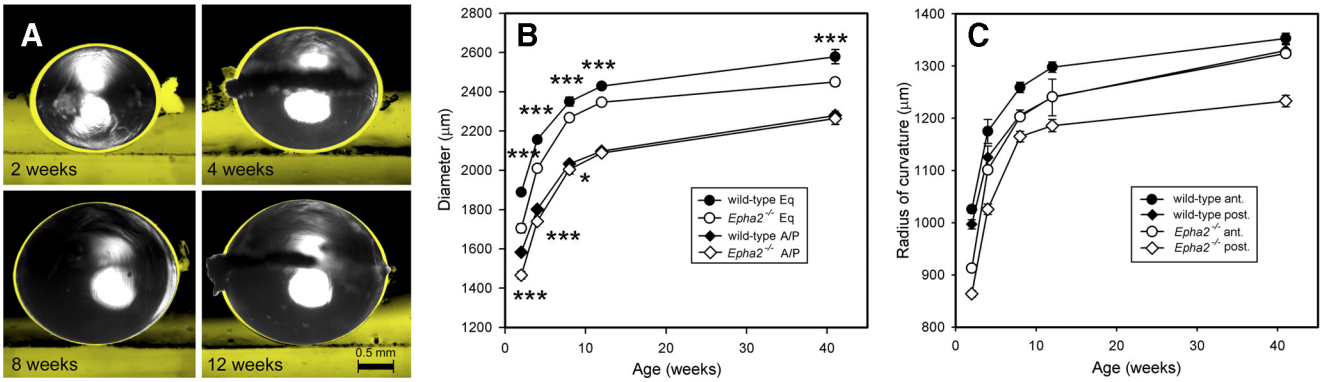

FIGURE 3. Comparative analysis of size and shape in wild-type and *Epha2*$^{-/-}$ lenses. (**A**) Lenses were suspended in tissue culture medium containing 20% Percoll and oriented with the anterior surface down. Wild-type lenses (*yellow silhouettes*) are larger at all ages, an effect most pronounced in lenses of young (2-week-old) mice. (**B**) Growth of wild-type and *Epha2*$^{-/-}$ lenses in the anterior/posterior (A/P) and equatorial (Eq) axes. (**C**) Change in the curvature of the anterior (ant.) or posterior (post.) lens surfaces with aging. (**B**, **C**) Data represent mean ± SD (n = 3). Statistical significance (two-way ANOVA): $^{*}P \leq 0.05$; $^{**}P \leq 0.01$; $^{***}P \leq 0.001$.

the underlying grid pattern) were observed consistently in young lenses, becoming more pronounced with age. In 10-month-old animals, two well-defined refractive compartments were present, an outer layer (approximately 0.2 mm thick) and a central region composing the remainder of the radius (Fig. 4A). To quantify differences in refractive properties, a laser beam was stepped in regular increments across the lens. The refracted beams were photographed and collected into a composite image (Fig. 4B). The focal length (back vertex distance) and angle of refraction were measured for each beam position (Figs. 4C and 4D, respectively). The most striking differences in refractive properties between the two genotypes were observed in the outer layers of the lens. Beams directed through the periphery of *Epha2*$^{-/-}$ lenses were less strongly refracted than those passing through equivalent regions of wild-type lenses.

Position, Shape, and Orientation of Lens Sutures

The coordinated elongation and migration of cohorts of lens fiber cells resulted in the convergence of the fiber cell tips beneath the anterior and posterior poles of the lens, at virtual

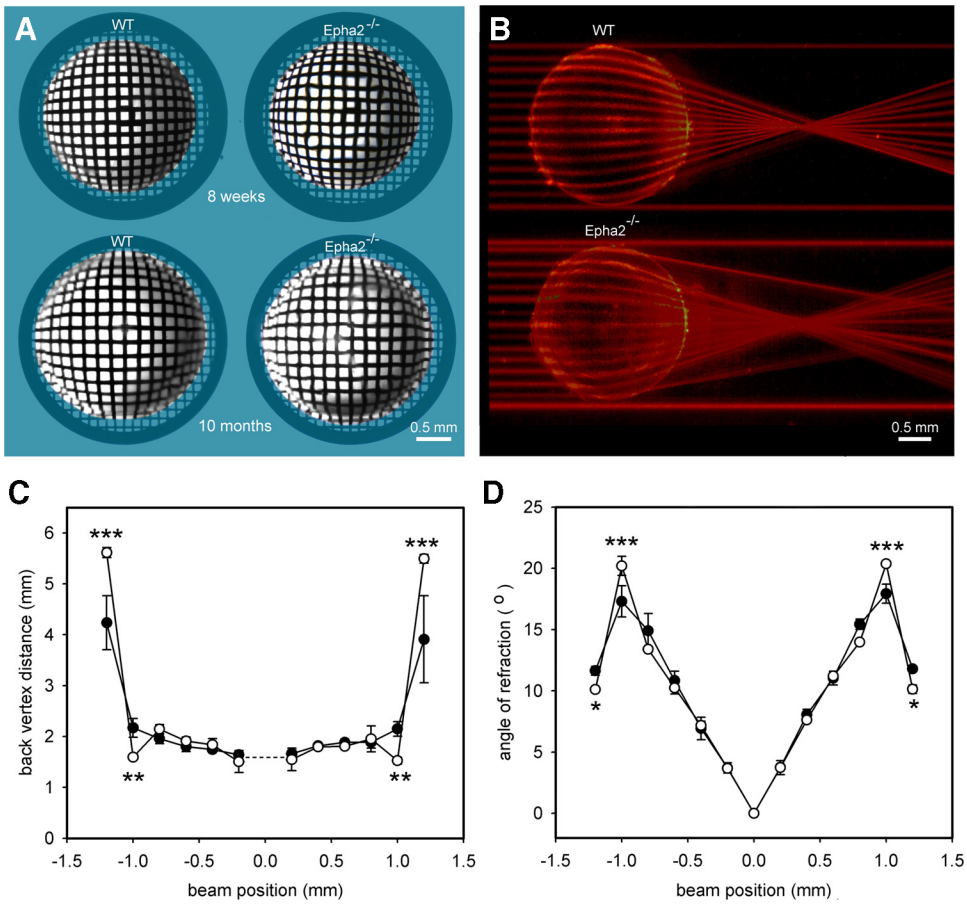

FIGURE 4. Refractive properties of wild-type and *Epha2*$^{-/-}$ lenses. (**A**) 8-week-old or 10-month-old wild-type and *Epha2*$^{-/-}$ lenses were photographed against a grid pattern. All lenses are transparent, but the grid image is distorted in *Epha2*$^{-/-}$ lenses. (**B**) Laser beams directed through the periphery of *Epha2*$^{-/-}$ lenses are less strongly refracted than through equivalent regions of wild-type lenses. (**C**) Focal length (back vertex distance) as a function of beam eccentricity. (**D**) Refractive angle as a function of beam eccentricity. (*open symbols*) Data from *Epha2*$^{-/-}$ lenses. (*closed symbols*) Wild-type data. Data represent mean ± SD (n = 3). Statistical significance (two-way ANOVA): $^{*}P \leq 0.05$; $^{**}P \leq 0.01$; $^{***}P \leq 0.001$.

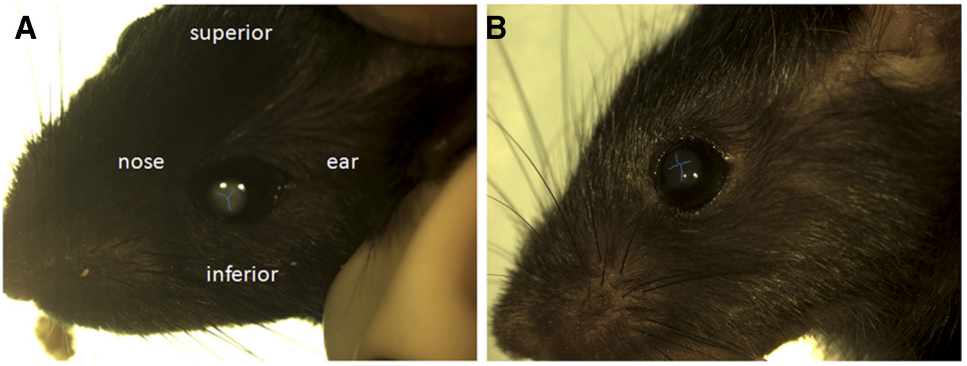

FIGURE 5. Orientation of the anterior sutures in 2-month-old wild-type or *Epha2*$^{-/-}$ mice. In wild-type mice (**A**), the anterior suture has an upright Y-shape. In *Epha2*$^{-/-}$ animals (**B**), the anterior suture is misshapen and is not oriented with respect to the superior/inferior axis of the head. To aid in visualization, the sutures are highlighted in *blue*.

structures called lens sutures.[24] In many mammals, lens sutures have a distinctive Y-shape, with rotational symmetry and 120° separation among the three suture branches. The sutures are centered on the optic axis and oriented with respect to the superior/inferior axis of the head. The posterior suture is usually smaller than the anterior suture and inverted with respect to the anterior suture. Thus, lens sutures have a characteristic form, position, and orientation that reflect the coordinated movement of differentiating fiber cells. We examined these morphologic parameters in lenses from wild-type and *Epha2*$^{-/-}$ mice.

In euthanized animals, with suitable lighting the anterior suture was visible through the cornea as a faint, bifurcated line on the front surface of the lens (Fig. 5). In wild-type mice, the anterior suture had a characteristic Y-shape. The point of intersection of the three suture branches was centered on the optic axis. The suture was rotated such that the Y-shape was upright with respect to the superior/inferior axis of the head and the stem of the Y was usually slightly longer than the branches. In contrast, the anterior suture of *Epha2*$^{-/-}$ animals was usually not Y-shaped, generally not centered on the optic axis, and showed no obvious orientation with respect to the superior/inferior axis of the head. The posterior sutures were usually not visible in situ using this technique.

To examine the spatial relationship between the anterior and posterior sutures in greater detail, lenses were removed from the eyes and incubated with FM 4-64, a fluorescent dye that stains the plasma membranes of the lens fiber cells and has been used previously to visualize suture architecture.[22] A gallery of projections of anterior and posterior sutures is shown in Figure 6. There was some variability in suture organization in wild-type lenses (Figs. 6A–D). Occasionally, for example, a branch of the anterior suture showed a secondary bifurcation, generating an "H-shaped" structure. In general, however, in wild-type lenses, the anterior and posterior sutures were symmetrical Y-shapes with straight branches and the sutures were centered on the optic axis. The posterior suture was smaller than the anterior suture and always inverted with respect to the anterior suture. In *Epha2*$^{-/-}$ animals, lens sutures were profoundly disturbed (Figs. 6E–H). Often the sutures, particularly the posterior sutures, were not Y-shaped. If a suture had a Y-shaped configuration, the branches of the Y were usually not straight, not of equal length, and not rotationally symmetric (i.e., the suture branches were not separated by 120°). Furthermore, the sutures were not centered on the optic axis, and the posterior suture was not oriented appropriately with respect to the anterior suture.

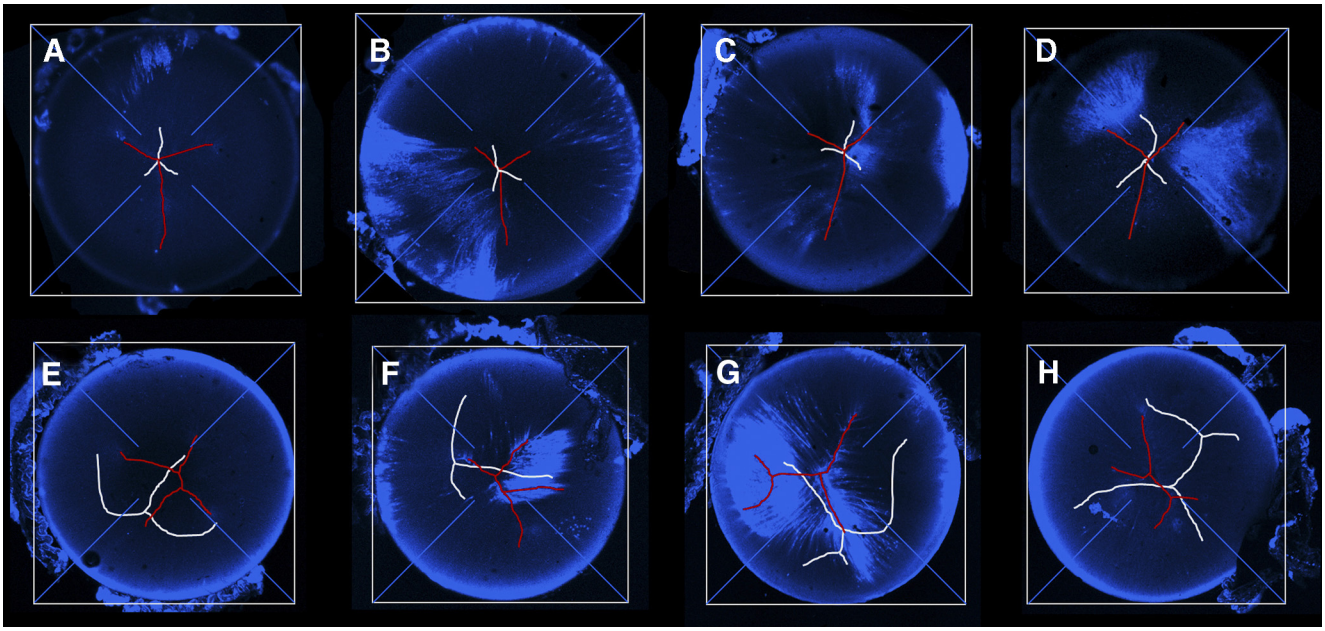

FIGURE 6. Gallery of images showing lens suture organization in 8-week-old wild-type (**A–D**) and *Epha2*$^{-/-}$ (**E–H**) mice. Anterior sutures are shown in *red* and posterior sutures in *white*. The optical axis is located at the convergence of the crosshairs. Images are maximum intensity orthographic projections of FM 4-64–stained lenses. In wild-type lenses, the sutures are located on the optic axis and have a characteristic Y-configuration. In contrast, sutures in *Epha2*$^{-/-}$ animals are not centered on the optic axis and exhibit a range of aberrant morphologies.

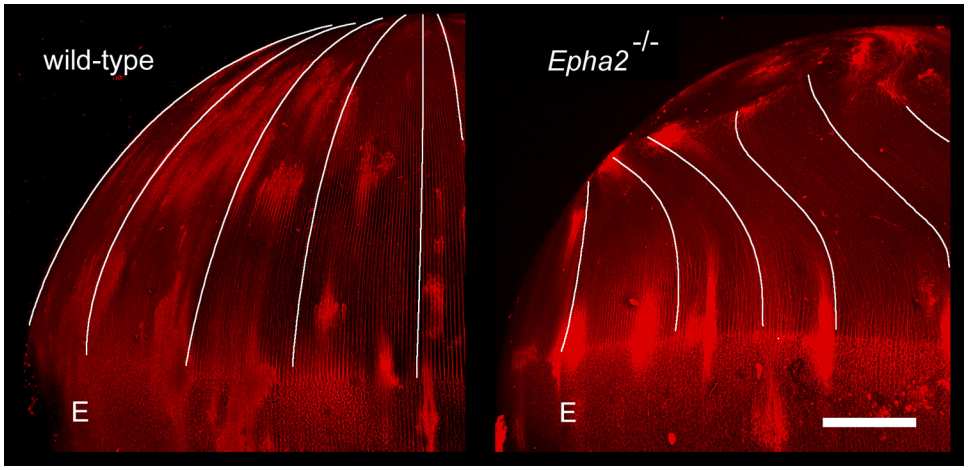

FIGURE 7. Aberrant fiber cell migration in *Epha2*$^{-/-}$ lenses. Two-month-old lenses were stained with FM 4-64 and were visualized in the equatorial aspect by confocal microscopy. In wild-type lenses, fiber cells project toward the posterior pole. In contrast, *Epha2*$^{-/-}$ fiber cells deviate from their normal course, curving away from the pole and terminating at mislocalized posterior suture branches. E, epithelium. Scale bar, 250 μm.

Distortions in suture shape and orientation signified that *Epha2*$^{-/-}$ fiber cells no longer followed their usual course during the cellular elongation process. Equatorial projections of FM 4-64–stained lenses revealed that rather than extending toward the poles, *Epha2*$^{-/-}$ fiber cells followed a tangential path before terminating off-axis at mislocalized sutures (Fig. 7). High-magnification images of fiber cells converging on the sutures confirmed that the regular packing of fiber cells characteristic of wild-type lenses is disturbed in *Epha2*$^{-/-}$ lenses (Supplementary Fig. S4, http://www.iovs.org/lookup/suppl/doi:10.1167/iovs.11-8568/-/DCSupplemental).

Individual fiber cells were dissected from wild-type or *Epha2*$^{-/-}$ lenses and visualized by confocal microscopy. Image stacks were deconvolved and rendered in three dimensions (Fig. 8). Fiber cells from wild-type lenses had a flattened hexagonal cross-sectional profile. The lateral membrane had six faces: two broad faces (oriented parallel to the lens surface) and four narrow faces. Membrane protrusions extended from the cell vertices. Wild-type cortical lens fiber cells had an undulating aspect when viewed from the broad side. Surface patterning of *Epha2*$^{-/-}$ fiber cells was disturbed. Membrane protrusions were not restricted to the cell vertices but instead extended from all membrane surfaces. *Epha2*$^{-/-}$ fiber cells also lacked the undulating morphology of wild-type fibers.

Epithelial Lesions

A consistent feature of *Epha2*$^{-/-}$ lenses was the presence of epithelial lesions at the anterior surface. Such structures were not observed in wild-type lenses. By adjusting the lighting conditions, lesions were visible in fresh tissue as small, refractive structures located immediately beneath the anterior surface of the lens (data not shown). Viewed en face, the lesions were circular and measured 50 to 100 μm in diameter. Lesions were observed in >50% of *Epha2*$^{-/-}$ lenses and were variable in number, ranging from 0 to 17 lesions per lens (Supplementary Fig. S5, http://www.iovs.org/lookup/suppl/doi:10.1167/iovs.11-8568/-/DCSupplemental). The lesions were not more numerous in older lenses than in younger lenses, appeared to be randomly distributed, and were present at all latitudes of the epithelium from the anterior pole to the equator. There was no apparent spatial relationship between the lesions and the underlying branches of the anterior suture. In three-dimensional reconstructions of EdU-labeled, Draq5-stained lenses, lesions were evident as gaps in the otherwise uniform field of epithelial nuclei (Fig. 9). The lesions were not associated with local zones of increased cell proliferation (Fig. 9A). Although the images of Draq5-stained nuclei suggested that lesions might represent breaks in the epithelial monolayer, staining of live, organ-cultured lenses with the lipophilic membrane probe FM 4-64 demonstrated that epithelial integrity was preserved in *Epha2*$^{-/-}$ lenses (Figs. 9B–D). FM 4-64 staining also revealed that the lesions had an unusual structure, consisting of a membranous dome above a shallow depression in the lens epithelium (Figs. 9C, 9D). The dome projected far into the lens capsule, the enveloping collagenous basement membrane of the lens. Although there were no nucleated cells in the region of the lesion, epithelial integrity was preserved because portions of the neighboring nucleated epithelial cells extended beneath the dome (Fig. 9D).

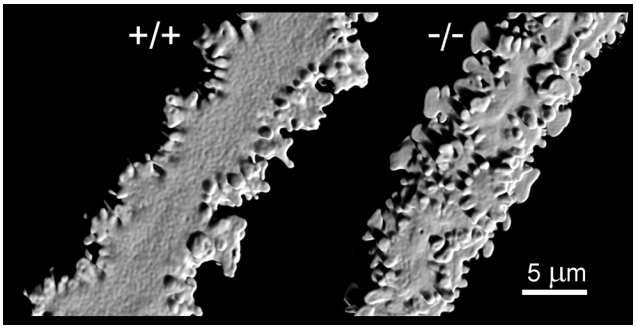

FIGURE 8. Single-cell confocal imaging reveals morphologic defects in individual *Epha2*$^{-/-}$ cortical fiber cells of 1-month-old lenses. Wild-type fiber cells follow an undulating course. Membrane protrusions extend from the short sides of the lateral membrane. *Epha2*$^{-/-}$ cells do not undulate, and protrusions project from all surfaces of the lateral membrane.

Discussion

The ability of the lens to form a sharply focused image on the retina is a function of its shape and internal composition. Our data show that Epha2 has a profound influence on both these parameters. In the absence of Epha2, the equatorial lens diameter was reduced by 5% to 10% at all ages, resulting in mutant mouse lenses that were more spherical than age-matched wild-type lenses. Laser analysis also revealed a decrease in the refractive power of the outer cell layers of *Epha2*$^{-/-}$ lenses. Lens cells contain extraordinary concentrations (500 mg/mL) of soluble proteins called crystallins that confer the necessarily high refractive index on the cells. The concentration of crystallin proteins varies with radial position. Cells located in the center of the lens have significantly higher protein contents than those situated near the

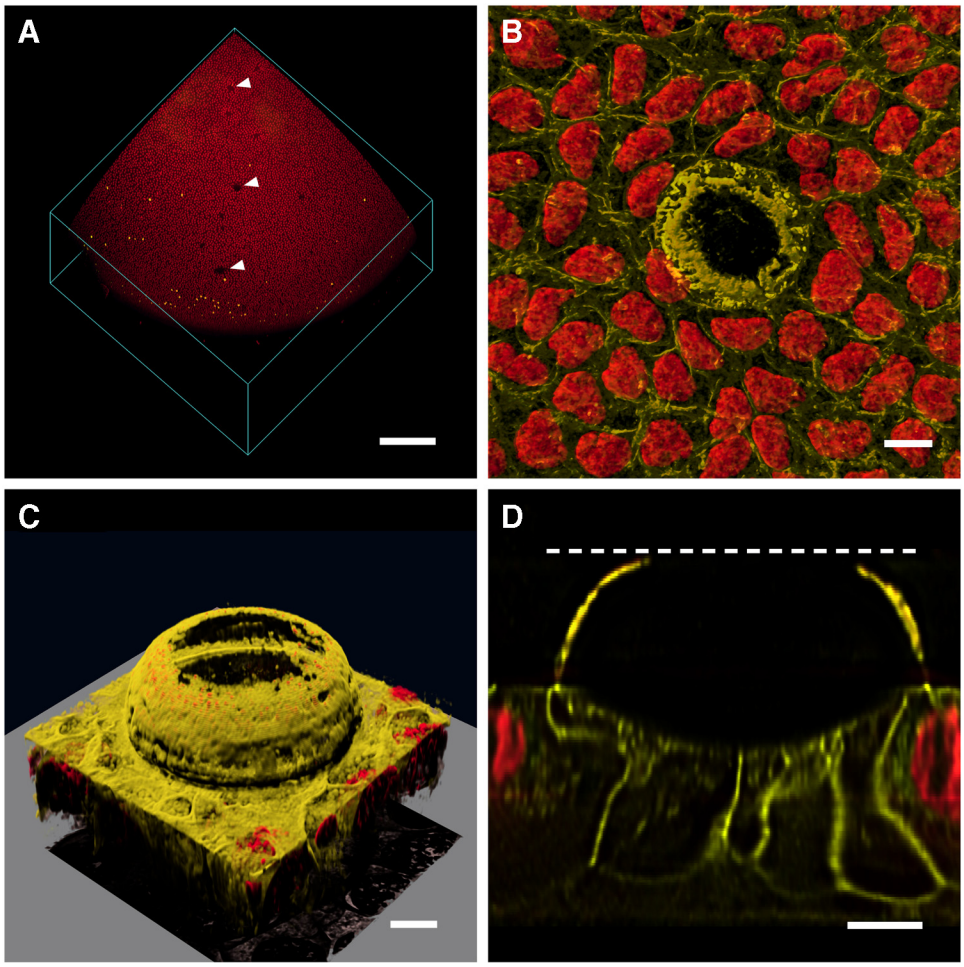

FIGURE 9. Lesions in the lens epithelium of *Epha2*$^{-/-}$ mice. (**A**) 3D rendering of an anterior lens quadrant. Note EdU-positive nuclei (*yellow*) located near the lens equator and gaps (*arrow*) in the Draq5-stained nuclear field (*red*). (**B**) Individual lesion visualized with a membrane stain, FM 4-64 (*yellow*), and Draq5 (*red*). (**C**) Oblique view of an epithelial lesion showing domelike membrane protrusion extending into the anterior lens capsule. (**D**) Orthogonal plane through the lesion shown in **C**. Nuclei are excluded from beneath the dome structure, but projections from neighboring epithelial cells maintain epithelial integrity beneath the dome. *Dashed line*: position of the capsule surface. Scale bars: 250 μm (**A**); 10 μm (**B**–**D**).

surface.[25] Paralleling this protein gradient is a refractive index gradient[26] that serves to correct longitudinal spherical aberration. Despite its central importance to the optics of the eye, little is known about how the refractive index gradient is generated in the lens and adjusted over the lifespan to match the refractive needs of the animal. The disturbed refractive properties of *Epha2*-null lenses suggest that this gene is involved in the establishment or maintenance, or both, of the gradient index.

Although the refractive properties of *Epha2*$^{-/-}$ lenses were disturbed, the tissue remained transparent. This finding conflicts with that of an earlier report, in which disruption of the *Epha2* locus in mice using a secretory gene-trapping strategy resulted in progressive cortical cataract formation.[15] In those animals, microscopic cellular disruptions were visible at 2 weeks. The incidence of cataract increased from 26% at 5 months of age to 83% by 14 months. Mature cataracts often featured frank rupture of the posterior capsule and extrusion of lens material. In the present study, we examined >100 lenses from *Epha2*$^{-/-}$ animals ranging from P2 to 1 year of age and did not observe cataracts. Occasionally, small flecklike opacities were present in the lens nucleus, but the incidence of such opacities was not greater in *Epha2*$^{-/-}$ lenses than in age-matched wild-type controls. The present data suggest that *Epha2* is not required for lens transparency, at least not on the mixed genetic background used here. The discrepancy between our findings and those in the previous study may reflect differences in genetic background. Several inbred strains of mice (e.g., 129) harbor mutations in the *Bfsp2* gene, which encodes CP49, an intermediate filament protein with important structural roles in the lens.[27] Lenses lacking CP49 are more fragile and prone to damage than wild-type lenses.[28] We excluded the *Bfsp2* mutation from our mice, but it is not clear from the methodological description of mice used in the earlier studies whether the *Bfsp2* mutation was present. The cataract-prone strain used previously (Epha2$^{Gt(KST085)Byg}$) was generated with the secretory gene trap approach. In that strategy, a fusion protein comprising a portion of the Epha2 ectodomain (encoded by exons 1–5) fused to a neomycin/β-galactosidase reporter cassette was trapped within the secretory pathway.[29] It is possible that the presence of the fusion protein could have contributed to the severity of the lens phenotype. In the present study, *Epha2* was disrupted by vector insertion into exon 5, introducing an in-frame translational stop codon within the vector sequence. It is unlikely that such a severely attenuated sequence would be translated, and neither of the antibodies used in the study detected Epha2 protein expression in the knockout mice. If a truncated mutant protein were to be translated, it is predicted to lack the transmembrane domain, the kinase domain, and the SAM (sterile alpha motif) domain of wild-type Epha2.

The presence of lesions in the anterior epithelium was a consistent aspect of the *Epha2*$^{-/-}$ lens phenotype. Three-dimensional imaging revealed the presence of domelike membranous structures overlying shallow depressions in the lens epithelium. These epithelial lesions may correspond to "subcapsular vacuoles" reported in an earlier study, although on slit-lamp examination those structures were deemed to be located in the anterior lens cortex rather than the epithelium.[15] If the two structures are equivalent, how-

ever, it would suggest that unlike lens opacification, epithelial lesions represent a consistent, strain-independent feature of the phenotype. The significance of the lesions, however, is uncertain.

The sutural defects and disturbances in the surface patterning of individual fiber cells observed in *Epha2*$^{-/-}$ lenses may imply that Epha2 has a role in the directed migration of lens fiber cells. The lens is an exquisitely patterned structure. Differentiating lens fiber cells undergo an enormous (10^2- to 10^3-fold) and rapid (up to 140 μm/d) increase in cell length.[30] During fiber cell elongation, cell tips follow a proscribed route beneath the lens epithelium (anteriorly) and the lens capsule (posteriorly). The convergence of the fiber tips results in the formation of virtual structures called sutures. The sutures have a characteristic form and orientation that reflect the coordinated elongation of cohorts of lens fiber cells. Although suture formation is central to the establishment of the lens cytoarchitecture, little is known about the underlying signaling mechanisms, though current data suggest that *Epha2* is implicated in this process.

The ligand or ligands for Epha2 in the lens are unknown. However, it has recently been shown that mice lacking ephrin-a5 (Efna5) develop cataract and that the Epha2 receptor is hypophosphorylated in Efna5-null lenses, consistent with the notion that Efna5 serves as a physiological ligand.[31] In the generation of topographic maps in the developing nervous system, repulsive interactions between Efna ligands and Epha receptors help guide axonal growth cones toward appropriate targets.[32] Modulation of the neuronal actin cytoskeleton occurs through the neuronal guanine nucleotide exchange factor (Ngef)[33] and the downstream activation of RhoA signaling. It is possible that signaling through the Epha2 receptor plays an analogous role in cell guidance in the lens. Interestingly, the lens is one of very few nonneuronal tissues to express high levels of Ngef,[34] and inhibition of Rho signaling in the lens results in abnormal fiber cell migration and cytoskeletal disorganization.[35,36]

Acknowledgments

The authors thank Frank Schottler for help with assembling the laser refractometer and Jennifer King-Sitzes and Seta Dikranian for technical assistance.

References

1. Pitulescu ME, Adams RH. Eph/ephrin molecules—a hub for signaling and endocytosis. *Genes Dev.* 2010;24:2480–2492.
2. Pasquale EB. Eph-ephrin bidirectional signaling in physiology and disease. *Cell.* 2008;133:38–52.
3. Hirai H, Maru Y, Hagiwara K, Nishida J, Takaku F. A novel putative tyrosine kinase receptor encoded by the *eph* gene. *Science.* 1987; 238:1717–1720.
4. Unified nomenclature for Eph family receptors and their ligands, the ephrins: Eph Nomenclature Committee. *Cell*. 1997;90:403–404.
5. Himanen JP, Chumley MJ, Lackmann M, et al. Repelling class discrimination: ephrin-A5 binds to and activates EphB2 receptor signaling. *Nat Neurosci.* 2004;7:501–509.
6. Lindberg RA, Hunter T. cDNA cloning and characterization of eck, an epithelial cell receptor protein-tyrosine kinase in the eph/elk family of protein kinases. *Mol Cell Biol.* 1990;10:6316–6324.
7. Mori T, Wanaka A, Taguchi A, Matsumoto K, Tohyama M. Differential expressions of the eph family of receptor tyrosine kinase genes (sek, elk, eck) in the developing nervous system of the mouse. *Brain Res Mol Brain Res.* 1995;29:325–335.
8. Easty DJ, Guthrie BA, Maung K, et al. Protein B61 as a new growth factor: expression of B61 and up-regulation of its receptor epithelial cell kinase during melanoma progression. *Cancer Res.* 1995; 55:2528–2532.
9. Walker-Daniels J, Coffman K, Azimi M, et al. Overexpression of the EphA2 tyrosine kinase in prostate cancer. *Prostate.* 1999;41:275–280.
10. Zelinski DP, Zantek ND, Stewart JC, Irizarry AR, Kinch MS. EphA2 overexpression causes tumorigenesis of mammary epithelial cells. *Cancer Res.* 2001;61:2301–2306.
11. Bassnett S, Wilmarth PA, David LL. The membrane proteome of the mouse lens fiber cell. *Mol Vis.* 2009;15:2448–2463.
12. Shiels A, Bennett TM, Knopf HL, et al. The *EPHA2* gene is associated with cataracts linked to chromosome 1p. *Mol Vis.* 2008;14: 2042–2055.
13. Zhang T, Hua R, Xiao W, et al. Mutations of the *EPHA2* receptor tyrosine kinase gene cause autosomal dominant congenital cataract. *Hum Mutat.* 2009;30:E603–E611.
14. Kaul H, Riazuddin SA, Shahid M, et al. Autosomal recessive congenital cataract linked to EPHA2 in a consanguineous Pakistani family. *Mol Vis.* 2010;16:511–517.
15. Jun G, Guo H, Klein BEK, et al. EPHA2 is associated with age-related cortical cataract in mice and humans. *PLoS Genet.* 2009;5.
16. Tan W, Hou S, Jiang Z, Hu Z, Yang P, Ye J. Association of EPHA2 polymorphisms and age-related cortical cataract in a Han Chinese population. *Mol Vis.* 2011;17:1553–1558.
17. Brantley-Sieders DM, Caughron J, Hicks D, Pozzi A, Ruiz JC, Chen J. EphA2 receptor tyrosine kinase regulates endothelial cell migration and vascular assembly through phosphoinositide 3-kinase-mediated Rac1 GTPase activation. *J Cell Sci.* 2004;117: 2037–2049.
18. Alizadeh A, Clark J, Seeberger T, Hess J, Blankenship T, FitzGerald PG. Characterization of a mutation in the lens-specific CP49 in the 129 strain of mouse. *Invest Ophthalmol Vis Sci.* 2004; 45:884–891.
19. De Maria A, Shi Y, Luo X, Van Der Weyden L, Bassnett S. Cadm1 expression and function in the mouse lens. *Invest Ophthalmol Vis Sci.* 2011;52:2293–2299.
20. Bassnett S, Shi Y. A method for determining cell number in the undisturbed epithelium of the mouse lens. *Mol Vision.* 2010;16: 2294–2300.
21. Bassnett S, Shi Y, Vrensen GF. Biological glass: structural determinants of eye lens transparency. *Philos Trans R Soc Lond B Biol Sci.* 2011;366:1250–1264.
22. Bassnett S, Shi YR, Barton K, De Maria A, Petrash JM, Shiels A. The stratified syncytium of the vertebrate lens. *J Cell Sci.* 2009;122: 1607–1615.
23. Bassnett S. On the mechanism of organelle degradation in the vertebrate lens. *Exp Eye Res.* 2009;88:133–139.
24. Kuszak JR, Zoltoski RK, Tiedemann CE. Development of lens sutures. *Int J Dev Biol.* 2004;48:889–902.
25. Palmquist BM, Philipson B, Fagerholm P. Nuclear cataract—a microradiographic study. *Acta Ophthalmol.* 1988;66:671–677.
26. Campbell MC. Measurement of refractive index in an intact crystalline lens. *Vision Res.* 1984;24:409–415.
27. FitzGerald PG, Fudge DS, McCuaig JV, et al. Intermediate filaments regulate tissue size and stiffness in the murine lens. *Invest Ophthalmol Vis Sci.* 2011;52:3860–3867.
28. FitzGerald PG, Yoon KH, Blankenship T, Shibata B. Resisting the effects of aging: a function for the fiber cell beaded filament. *Invest Ophthalmol Vis Sci.* 2008;49:1030–1036.
29. Skarnes WC, Mitchell KJ, Pinson KI, et al. Functional analysis of secreted and transmembrane proteins critical to mouse development. *Nat Genet.* 2001;28:241–249.
30. Bassnett S, Winzenburger PA. Morphometric analysis of fibre cell growth in the developing chicken lens. *Exp Eye Res.* 2003;76:291–302.
31. Zhou RP, Cooper MA, Son AI, Komlos D, Suna YH, Kleiman NJ. Loss of ephrin-A5 function disrupts lens fiber cell packing and leads to cataract. *Proc Natl Acad Sci USA.* 2008;105:16620–16625.
32. O'Leary DDM, Feldheim DA. Visual map development: bidirectional signaling, bifunctional guidance molecules, and competition. *Csh Perspect Biol.* 2010;2.
33. Greenberg ME, Sahin M, Greer PL, et al. Eph-dependent tyrosine phosphorylation of ephexin1 modulates growth cone collapse. *Neuron.* 2005;46:191–204.

34. Lattin JE, Schroder K, Su AI, et al. Expression analysis of G protein-coupled receptors in mouse macrophages. *Immunome Res.* 2008;4:5.
35. Maddala R, Deng PF, Costello JM, Wawrousek EF, Zigler JS, Rao VP. Impaired cytoskeletal organization and membrane integrity in lens fibers of a Rho GTPase functional knockout transgenic mouse. *Lab Invest.* 2004;84:679–692.
36. Maddala R, Reneker LW, Pendurthi B, Rao PV. Rho GDP dissociation inhibitor-mediated disruption of Rho GTPase activity impairs lens fiber cell migration, elongation and survival. *Dev Biol.* 2008; 315:217–231.
37. Brantley-Sieders DM, Zhuang G, Hicks D, et al. The receptor tyrosine kinase EphA2 promotes mammary adenocarcinoma tumorigenesis and metastatic progression in mice by amplifying ErbB2 signaling. *J Clin Invest.* 2008;118:64–78.
38. Shiels A, King JM, Mackay DS, Bassnett S. Refractive defects and cataracts in mice lacking lens intrinsic membrane protein-2. *Invest Ophthalmol Vis Sci.* 2007;48:500–508.